Climate Dynamics (2019) 52:913–927
https://doi.org/10.1007/s00382-018-4264-6

Modulation of tropical cyclone tracks over the western North Pacific by intra-seasonal Indo-western Pacific convection oscillation during the boreal extended summer

Qiuyun Wang[1] · Jianping Li[1,2] · Yanjie Li[3] · Jiaqing Xue[3,4] · Sen Zhao[5,6] · Yidan Xu[1] · Yuehong Wang[1] · Yazhou Zhang[1] · Di Dong[3,4] · Jingwen Zhang[7]

Received: 17 October 2017 / Accepted: 9 March 2018 / Published online: 26 May 2018

Abstract
This study investigates the effect of the intra-seasonal Indo-western Pacific convection oscillation (IPCO) on tropical cyclone (TC) tracks over the western North Pacific (WNP) during the boreal extended summer (May−October). The number of west- and northwest-moving TC tracks is found to sharply increase over the WNP in the positive intra-seasonal IPCO phase. Recurving tracks have greater weight in the negative intra-seasonal IPCO phase. Possible physical mechanisms are further examined in terms of steering flow, energy conversion, and energy propagation. When the intra-seasonal IPCO phase is positive, the first-order moment term of perturbation potential energy (PPE_1) converts into perturbation kinetic energy (PKE) at lower latitudes. The pressure trough spreads farther to the east. Meanwhile, Rossby waves emanating from the convective centers of the intra-seasonal IPCO over the WNP ($Wave_{WNP}$) and EEIO ($Wave_{EEIO}$) travel into the trough region, thereby deepening the trough. These features enhance the westward and northwestward steering flow between 20°N and about 30°N, sharply increasing the number of straight west- and northwest-moving TC tracks over the WNP. When the intra-seasonal IPCO is in a negative phase, conversion from PPE_1 to PKE at lower latitudes is suppressed and the trough weakens. More PPE_1 converts to PKE in the climatological western Pacific subtropical high (WPSH) region and the WPSH is intensified. Moreover, $Wave_{EEIO}$ intensifies the north–south ridge of the WPSH over the southern Indian Peninsula. Meanwhile, part $Wave_{WNP}$ propagate northeastward. These features favor northeastward motion of TCs over the WNP.

Keywords Intra-seasonal Indo-western Pacific convection oscillation · Tropical cyclone tracks · Western North Pacific · Perturbation potential energy · Rossby wave

1 Introduction

Tropical cyclone (TC) activities have an important impact on the safety and security of people of the affected areas (Emanuel 2005). The western North Pacific (WNP) basin is the most active region of TC genesis, generating more than 30% of TCs worldwide (Li et al. 2016b). The TC activity over the WNP has been the subject of much researches (e.g Chan 1995; Wang and Chan 2002; Emanuel 2003; Camargo and Sobel 2005; Wang and Wang 2013; Zhan et al. 2011a,

✉ Jianping Li
ljp@bnu.edu.cn

[1] College of Global Change and Earth System Sciences (GCESS), Beijing Normal University, Beijing 100875, China

[2] Laboratory for Regional Oceanography and Numerical Modeling, Qingdao National Laboratory for Marine Science and Technology, Qingdao 266237, China

[3] State Key Laboratory of Numerical Modeling for Atmospheric Sciences and Geophysical Fluid Dynamics (LASG), Institute of Atmospheric Physics, Chinese Academy of Sciences, Beijing 100029, China

[4] College of Earth Science, University of Chinese Academy of Sciences, Beijing 100049, China

[5] Key Laboratory of Meteorological Disaster of Ministry of Education, College of Atmospheric Science, Nanjing University of Information Science and Technology, Nanjing 210044, China

[6] Department of Atmospheric Sciences, University of Hawai'i at Mānoa, Honolulu, HI 96822, USA

[7] Chengdu Meteorological Bureau, Chengdu 610072, China

b, 2014; Wang et al. 2014; Choi et al. 2016; Kim et al. 2016; Li et al. 2016a). The challenge for future projections of TC activity is not only to develop a reliable projection of changes in the various factors influencing TCs, but also to find a means of simulating the effect of these climate changes on TC metrics such as TC frequency, intensity, and tracks (Knutson et al. 2010). The dominant tropical intra-seasonal oscillation (ISO) is known as the Madden–Julian oscillation (MJO). Gray (1979) was the first to investigate a possible linkage between the MJO and global TC activity, revealing that TC genesis tends to be clustered over a period of 2–3 weeks around the globe. Subsequently, an increasing number of studies have focused on the relationship between the MJO and TC activity, especially in the WNP. TC activity shows significant clustering and periodicity on intra-seasonal timescales (e.g Maloney and Hartmann 2000a, b; Sobel and Maloney 2000; Hartmann and Maloney 2001; Zhu et al. 2004). In addition, TC tracks show significant intra-seasonal variability (e.g Harr and Elsberry 1991, 1995; Kim et al. 2008; Chen et al. 2009; Li and Zhou 2013).

Convective activity exhibits a feature of ISO in the tropics. There is a convective seesaw over the Indo-western Pacific on intra-seasonal timescales (Lau and Chan 1986; Zhu and Wang 1993). This out-of-phase fluctuation of convection anomalies over the Indo-western Pacific is also evident in the seasonal and annual mean states, as reported by Li et al. (2013), who used the term Indo-western Pacific Convection Oscillation (IPCO). More recently, Zhang et al. (2015) introduced the concept of the IPCO for intra-seasonal timescales and found that this out-of-phase convection oscillation exists throughout the entire year; they called this feature the intra-seasonal IPCO. The average locations of the convection centers of the intra-seasonal IPCO lie over the equatorial eastern Indian Ocean (EEIO) (5°S–10°N, 70°–100°E) and the WNP (5°–20°N, 110°–160°E). The propagation of the intra-seasonal IPCO is divided into two branches: one propagates eastward from the NIO (north Indian Ocean) to the WNP, and is suppressed temporarily as it passes over the Maritime Continent and then strengthens and turns northward over the WNP. And another one propagates northward from the equatorial Indian Ocean to the Indian Peninsula (Zhang et al. 2015). The classical MJO cannot capture this northward propagating characteristic (Wheeler and Hendon 2004; Ding et al. 2011). The intra-seasonal IPCO also has a non-propagating part. The propagating part of the intra-seasonal IPCO during the boreal extended summer (May–October) is closely connected with the propagation of the boreal summer ISO (Kikuchi et al. 2012). The intra-seasonal IPCO has an important effect on the climate and weather events over the Indo-western North Pacific, and indeed on TC activity (Li et al. 2013). Wang et al. (2017) reported that the impacts of the intra-seasonal IPCO on TCs over the Indo-western North Pacific (Indo-WNP) include an evident "phase lock of TC genesis location" and distinct differences in TC frequency during the boreal extended summer in the period 1979–2015. In addition to the frequency and location of TC genesis, the TC track is one of essential metric of TC activity. And TC track forecast is also an important part of TC forecasts. Does the intra-seasonal IPCO have an impact on TC tracks over the WNP, and if so, what is the mechanism? In this work, we will answer these two questions.

The remainder of this paper is organized as follows: Sect. 2 provides a brief review of the data and analysis methods. In Sect. 3, the statistical characteristics of TC tracks in the positive and negative intra-seasonal IPCO phases are presented, and Sect. 4 discusses the physical mechanisms that underlie the differences in TC tracks in the various phases. Finally, the key results and conclusions are presented in Sect. 5.

2 Data and methodology

2.1 Data

Best-track data for TC activity over the WNP during 1979−2015 are obtained from the Regional Specialized Meteorological Center (RSMC) of the Japan Meteorological Agency (JMA, available online at http://www.jma.go.jp/jma/jma-eng/jma-center/rsmc-hp-pub-eg/trackarchives.html). Only TCs that reach tropical storm intensity (maximum sustained 10 m wind speed ≥ 17.2 m/s) are employed. The article employs daily datasets (including horizontal wind fields, pressure, vertical velocity, geopotential height, relative humidity, and air temperature) with 2.5° horizontal resolution during the boreal extended summer of 1979−2015 from the National Centers for Environmental Prediction and Atmospheric Research (NCEP/NCAR) reanalysis 1 data (Kalnay et al. 1996). Specific cloud liquid water content data with 2.5 horizontal resolution from the European Centre for Medium-Range Weather Forecasts Re-Analysis (ERA) Interim datasets are also used (Dee et al. 2011).

2.2 Statistical methods

Based on a previous study (Li et al. 2013; Zhang et al. 2015), the intra-seasonal IPCO index is given as

$$\mathrm{IPCOI} = \mathrm{OLR}_{\mathrm{EEIO}} - \mathrm{OLR}_{\mathrm{WNP}}, \quad (1)$$

where $\mathrm{OLR}_{\mathrm{EEIO}}$ and $\mathrm{OLR}_{\mathrm{WNP}}$ are the normalized 30−60-day bandpass-filtered area-averaged time series of OLR anomalies over the EEIO (5°S−10°N, 70°−100°E) and WNP (5°–20°N, 110°−160°E), respectively. An absolute value of IPCOI of between −1 and +1 is used to define a neutral phase of the IPCO, while values less than −1 define the

negative phase, and values greater than + 1 define the positive phase. A 30–60-day Lanczos bandpass filter using 139 weights is applied to the anomalies of the aforementioned meteorological elements, except the TC data.

Lead–lag correlation analysis is applied to examine the relation between the intra-seasonal IPCO and the western Pacific subtropical high (WPSH). A WPSH index is given by the normalized sum of the difference in geopotential height between each grid point at 700 hPa and 3160 gpm after applying a 30–60-day Lanczos bandpass filter. The statistical significance of the correlation between two autocorrelated time series is assessed via a two-tailed Student's *t*-test using the effective number of degrees of freedom (N_{eff}). N_{eff} is given by the following approximation (e.g Pyper and Peterman 1998; Li et al. 2012, 2013; Xie et al. 2014; Sun et al. 2015; Xue et al. 2017):

$$\frac{1}{N^{eff}} \approx \frac{1}{N} + \frac{2}{N}\sum_{j=1}^{N}\frac{N-j}{N}\rho_{XX}(j)\rho_{YY}(j), \tag{2}$$

where N is the sample size and $\rho_{XX}(j)$ and $\rho_{YY}(j)$ are the autocorrelations of the two sampled time series X and Y at time lag j, respectively. Composite analysis is employed to explore possible physical mechanisms.

2.3 Classification of TC tracks

To single TC, firstly, a straight line connecting TC genesis location and disappeared location is fixed. Table 1 present the classified method to TC tracks. If the obliquity (α, Fig. 1) of straight line relative to the equator is greater than or equal to 112.5° or the value of longitude at any time (excluding the last moment) is greater than or equal to one at the last moment, it will be identified as the west-moving or northwest-moving track (Table 1, categories III and II). Besides, west-moving track also include southwest-moving track (Table 1, category I). If α is less than 112.5° and the value of latitude at the last moment is greater than one at the genesis moment, it will be identified as recurving tracks (Table 1, categories I and II). Particularly, to a TC with turning point, if its meridional distance (difference in latitudes) from disappeared location to turning point is less than half zonal distance (difference in longitudes) from genesis location to turning point, and the zonal distance from disappeared location to turning point is less than 0.05 times zonal distance from genesis location to turning point, we think it belongs to the west- or northwest-moving tracks (Table 1, category IV).

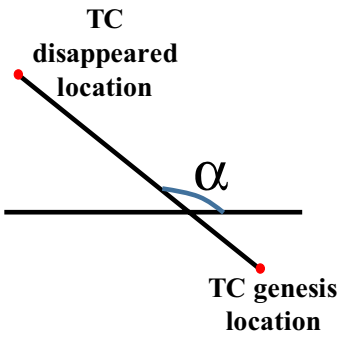

Fig. 1 The obliquity (α) of straight line relative to the equator. Straight line is defined by connecting TC genesis location (red dot) and disappeared location (red dot)

2.4 Vertical wind shear

According to the previous studies (Sharmila and Walsh 2017), we calculate the vertical wind shear (VWS) between adjacent atmospheric layers. VWS is defined as the magnitude of the vector different of wind between adjacent atmospheric layers:

$$VWS = \sqrt{\left(u_{ii+1} - u_{ii}\right)^2 + \left(v_{ii+1} - v_{ii}\right)^2}, \tag{3}$$

Table 1 The necessary conditions that different TC tracks need to meet

Conditions	West- and northwest-moving tracks				Recurving tracks	
	I	II	III	IV	I	II
$\alpha < 112.5°$	∅	∅	∅	Particularly, to a TC with turning point: $\lvert lat_i - lat_{turning\ point}\rvert < 0.5 \times \lvert lon_0 - lon_{turning\ point}\rvert$ and $\lvert lon_i - lon_{turning\ point}\rvert < 0.05 \times \lvert lon_0 - lon_{turning\ point}\rvert$	√	√
$\alpha \geq 112.5°$	∅	∅	√		∅	∅
$lon_0 \geq lon_i$	√	∅	∅		∅	∅
$All(lon_{0:i-1}) \geq lon_i$	∅	√	∅		∅	∅
$Any(lon_{0:i-1}) < lon_i$	∅	∅	∅		∅	√
$lat_0 < lat_i$	∅	∅	∅		√	√
$lat_0 \geq lat_i$	√	∅	∅		∅	∅

And lon represents longitude, lat latitude. Number 0 presents TC genesis moment, *i* disappeared moment. α indicates the obliquity of straight line (which connecting TC genesis location and disappeared location) relative to the equator. "√" represents condition which need to satisfy, "∅" represents condition which need not to satisfy

where u and v are zonal and meridional wind components, respectively; ii indicate one level of atmosphere.

2.5 Atmospheric perturbation potential energy (PPE)

A possible linkage between the energy and horizontal pressure distribution in a storm was first studied quantitatively by Margules (1903), who proposed the concept of atmospheric kinetic energy availability, which led to a focus on the atmospheric available potential energy (APE). Lorenz (1955) formulated the modern framework of atmospheric energetics. Subsequently, the theory of APE was continuously improved and has been employed in the energy analysis of atmospheric and oceanic processes (e.g Smith 1969; Smith et al. 1977; Xie 1978; Taylor 1979; Oort et al. 1989). However, the application of APE on regional energy conversion is limited, because the concept of APE is based on globally averaged variables (Gao and Li 2007, 2012; Li et al. 2016c; Dong et al. 2017). Through investigating some important characteristics of the atmosphere during an adiabatic process (Gao et al. 2006), Li and Gao (2006) proposed the perturbation potential energy (PPE) to express local APE. In isobaric coordinates, PPE (P'_{ai}) can be written as

$$P'_{ai} = \frac{p_{00}^{(i-1)\kappa}\prod_{j=0}^{i-1}(1+\kappa-j)}{i!\gamma_d(1+\kappa)}\int_0^{p_s}\frac{T'^i}{p^{(i+1)(1+\kappa)}}\left(-\frac{\partial\bar{\theta}}{\partial p}\right)^{-i+1}dp, \tag{4}$$

where i is the order of the PPE; p_{00} is a reference pressure (usually taken as 1000 hPa); $\gamma_d = g/c_p$ is the dry adiabatic lapse rate, where c_p is the specific heat at constant pressure and g is gravitational acceleration; $\kappa = R/c_p$ with R being the gas constant of dry air; p is pressure; p_s is surface pressure; T is temperature; and θ is potential temperature. In addition, T represents a global average on an isobaric surface and T′ the departure from this global average. The first-order PPE (PPE_1, P'_{a1}) and second-order PPE (PPE_2, P'_{a2}) are expressed as follows:

$$P'_{a1} = \frac{1}{\gamma_d}\int_0^{p_s} T'dp, \tag{5}$$

$$P'_{a2} = \frac{kp_{00}^k}{2\gamma_d}\int_0^{p_s}\frac{T'^2}{p^{1+k}}\left(-\frac{\partial\bar{\theta}}{\partial p}\right)^{-1}dp. \tag{6}$$

Li and Gao (2006) found that high-order moment terms of PPE are much smaller than PPE_1 and PPE_2, and can therefore be omitted. On a global average, PPE_1 diminishes, while PPE_2 become the major term, and the formula of PPE_2 is the same as APE. But there is a significant difference between PPE_2 and APE; i.e., the former is based on local regional variables, whereas the latter is based on globally averaged variables. Locally, PPE_1 is an order of magnitude larger than PPE_2; hence, we focus on PPE_1 in this study (The detailed governing equations of the atmospheric layer PPE_1 can be found in the Appendix A).

2.6 Non-stationary Rossby wave ray tracing method in the horizontal non-uniform basic flow

In order to understand how the intra-seasonal IPCO modulate tropical cyclone tracks from a perspective of energy propagation, non-stationary Rossby wave ray tracing method in horizontal non-uniform basic flow (details are shown in the Appendix B) is employed. Since the average TC life is 7–9 days and the convective oscillation has a period of 30–60 days, we set the initial zonal wavenumber to 1 and the period of the wave to 30 days in the different intra-seasonal IPCO phases.

3 TC tracks in the positive and negative intra-seasonal IPCO phases

As can be seen in Fig. 2 and Table 2, it is apparent that west- and northwest-moving tracks (accounting for ~ 56.5% of the total number) are more than recurving tracks (~ 41.8%) in a positive phase of the intra-seasonal IPCO. On the contrary, recurving tracks have greater weight (~ 54.4%) in the negative phase. In order to show the difference of TC tracks between the positive and negative intra-seasonal IPCO phases. We further explore the difference in frequency of TCs occurrence in each 2° latitude × 2° longitude grid between the positive and negative intra-seasonal IPCO phases and obtain the quantitative statistics of TCs tracks in two phases. As shown in the Fig. 3, straight west- and northwest-moving tracks sharply increase in the positive intra-seasonal IPCO phase compared with that in the negative phase over the WNP. Wang et al. (2017) reported that the total number of TC geneses over the WNP in the positive intra-seasonal IPCO phase is 2.16 times than that in its negative phase. By comparing the number of corresponding tracks in the two phases (Table 2), we find that there are 2.72 times as many west- and northwest-moving tracks (~ 166 TCs) in the positive phase than in the negative phase (~ 61 TCs). The number of recurving tracks in the positive phase (~ 123 TCs) is only 1.66 times that in the negative phase (~ 74 TCs). These figures implies that more TCs make landfall on the Indo-China Peninsula, eastern coastal China, and some islands in the South China Sea (SCS) during the positive intra-seasonal IPCO phase than during the negative

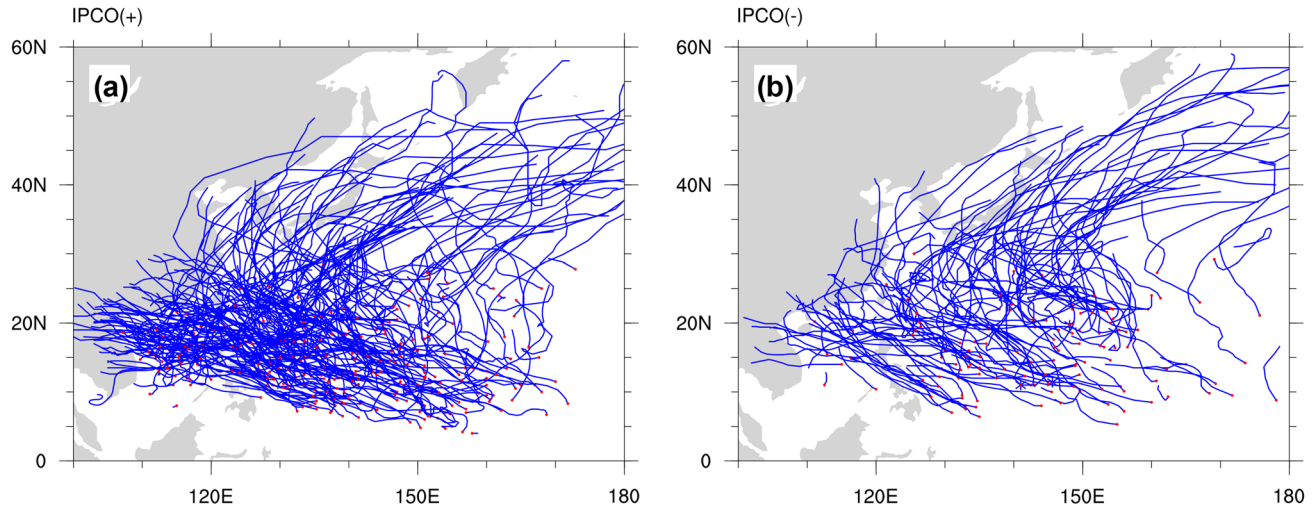

Fig. 2 TC tracks (blue lines) in the positive (**a**) and negative (**b**) intra-seasonal IPCO phases over the WNP in the boreal extended summer for the period 1979–2015. The red dots denote the TC genesis locations

Table 2 The quantitative statistics of TC tracks over WNP in boreal extended summer at positive and negative intra-seasonal IPCO phases (1979–2015)

Phase	Total number	Different tracks	Number	Proportion (%)
IPCO+	294	West- and northwest-moving tracks	166	56.5
		Recurving tracks	123	41.8
IPCO−	136	West- and northwest-moving tracks	61	44.9
		Recurving tracks	74	54.4

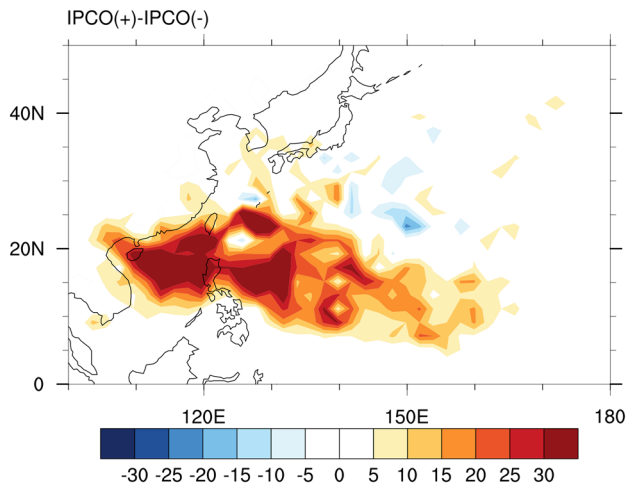

Fig. 3 Difference in frequency of TCs occurrence in each 2° latitude × 2° longitude grid between the positive and negative intra-seasonal IPCO phases over the WNP in the boreal extended summer for the period 1979–2015

phase. In addition, in order to further verify our results, we choose the four factors to represent TC tracks, including TC genesis locations, middle locations, disappeared locations and the mean of TC life periods of different tracks in two phases. Previous study (Wang et al. 2017) has shown that the statistic results of TC genesis locations is significantly different between the positive and negative phases, more TCs generate in the west of the WNP and at lower latitudes in the positive intra-seasonal IPCO than that in negative phase. Here, we just display the results of other three factors. Because there are tiny east- and southeast-moving TCs in the positive (about 5 TCs) and negative (only 1 TC) phases, we analyze total TCs locations at two phases. As shown in Table 3, TC mean middle and disappeared locations tend to migrate westward and southward in the positive phase, especially mean disappeared location (roughly 25.12°N, 132.82°E vs 28.73°N, 140.26°E in the negative phase). To the mean of TC life periods of different tracks in two phases, it is evident that the recurving tracks have longer life cycle in the negative phase compare with that in the positive phase. It implies TCs are easier to recurve to northward and northeastward in the negative phase than that in its positive phase. And there is no significant differences in life cycles of the west- and northwest-moving TCs between two phases, because of a limited distance from the TC genesis location to landing location. In general, the differences in these factors between the positive and negative phases are all evident, it

Table 3 The quantitative statistics of TC tracks factors (including TC middle locations, disappeared locations and mean of TC life period of different tracks) over the WNP in boreal extended summer at positive and negative intra-seasonal IPCO phases (1979–2015)

WNP			IPCO+	IPCO−
Total number of TC genesis			294	136
TC middle locations	Meridional	Mean	19.19°N**	21.57°N**
		Standard deviation	6.24°	7.13°
	Zonal	Mean	133.64°E**	138.56°E**
		Standard deviation	14.81°	14.82°
TC disappeared locations	Meridional	Mean	25.12°N**	28.73°N**
		Standard deviation	10.95°	12.7°
	Zonal	Mean	132.82°E**	140.26°E**
		Standard deviation	21.3°	22.91°
Mean of TC life period of different tracks (units: h)		West- and northwest-moving TCs	127.76	121.52
		Recurving moving TCs	171.39**	196.93**

One (two) asterisks indicate significance above the 90% (99%) confidence level using the Student's *t*-test

illustrates the differences in TC tracks between two phases are robust.

4 Possible physical mechanisms

4.1 Steering flow

TC tracks generally follow the steering flows (Chan 2010). A diagnostic horizon must be chosen to analyze the effect of steering flow on TC tracks. Figure 4 shows the vertical distribution of zonal mean kinetic energy and vertical wind shear between adjacent atmospheric layers. To the troposphere, it is evident from Fig. 4a that zonal mean kinetic energy at the 850−700-hPa levels is higher than that at other levels at low latitudes. Vertical wind shear remains weak around 700-hPa level (Fig. 4b), it supports the TC genesis and development, what's more, TC tracks is also related to the TC genesis and intensity (Yang et al. 2015). Therefore, combining these results with previous research (Chen et al. 2009), we choose to analyze the circulation fields at 700 hPa. As a large circulation feature in the WNP, the WPSH has an important effect on TC tracks. It is evident from Fig. 5 that a significant lead–lag relationship exists between the WPSH and the intra-seasonal IPCO. There is a significant negative correlation between the intra-seasonal IPCO and the WPSH when the change in the intra-seasonal IPCO leads the WPSH (negative lag), reaching a peak (around −0.366) at a lag of −7 days, indicating that the intra-seasonal IPCO has a dominant effect on the development of the WPSH. In contrast, there is a significant positive correlation between the intra-seasonal IPCO and the WPSH, when the change of the WPSH leads the intra-seasonal IPCO (positive lag), reaching a peak (around 0.375) at a lag of 14 days, suggesting a potential influence of

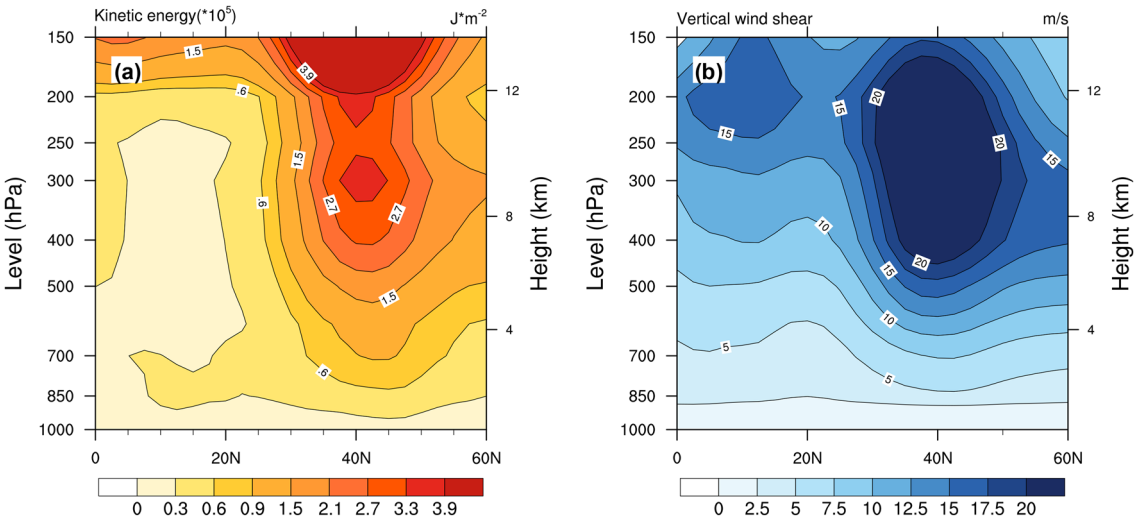

Fig. 4 Vertical distribution of zonal mean kinetic energy (**a**) and vertical wind shear between adjacent atmospheric layers (**b**) over the WNP in the boreal extended summer for the period 1979–2015

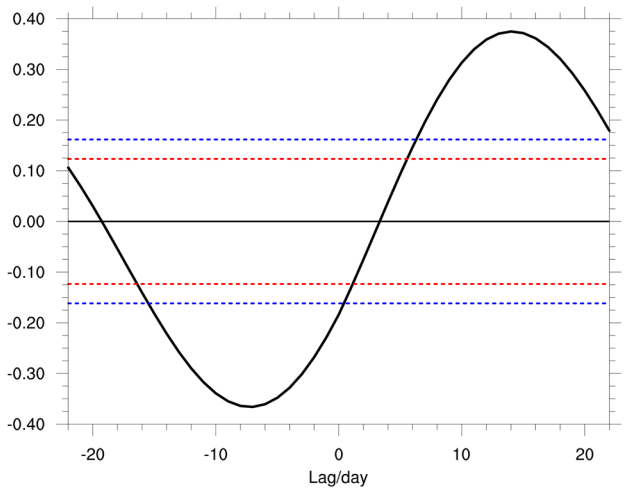

Fig. 5 Lead–lag relation between the intra-seasonal IPCO index and the WPSH index (negative lags denote the intra-seasonal IPCO leads the WPSH; vice versa). The dotted lines indicate significant at the 99% (blue) and 95% (red) confidence levels using Student's *t*-test, respectively

the WPSH on the intra-seasonal IPCO. Therefore, the intra-seasonal IPCO can affect TC tracks through the WPSH.

As shown in Fig. 6a, in the positive phase of the intra-seasonal IPCO, significant negative geopotential height anomalies occur in the region where the climatological trough is located over the WNP. As a result, the trough deepens, spreading farther to the east, further suppressing the development of the WPSH over the WNP (Fig. 7a). The ridge of the WPSH is farther north than in the negative phase (Fig. 7b), and the western edge of the 3160-gpm surface leans farther to the east. These features result in a change in the steering flow (Fig. 8a). With reference to Fig. 8a we can see there is anomalously cyclonic circulation in the positive intra-seasonal IPCO phase at low latitudes and west of 150°E in the WNP. And previous study (Wang et al. 2017) illustrates more TCs generate in the west of the WNP and at lower latitude, especially in the South China Sea (SCS). Although the anomalous eastward airflows occur in the WNP south of 17.5°N, not all anomalous westerlies are significant. Obvious anomalous westerlies occurs in the WNP south of 10°N and west of 140°E, which can suppress the westward and northwestward motion of TCs. However, there are only a few of TCs in these area. In the SCS, there are no obvious difference in TC tracks, because the center of anomalously cyclonic circulation is located here. To other regions where TCs mainly generate, there are not significant change of circulation, hence, most TCs move westward and northwestward because of β-effect. In addition, anomalous westward airflow about 10° poleward of 20°N can also prevent a northward and northeastward shift when the TCs move to the north of 20°N and west of 150°E. It is also the reason why the recurving tracks have shorter life cycle in the positive phase than that in its negative phases (Table 3). Most TCs make landfall on the Indo-China Peninsula, eastern coastal China, and some islands in the SCS during the positive phase.

In contrast, in the negative phase of the intra-seasonal IPCO, TC genesis locations is more dispersed and genesis region shifts to the east of the WNP (Wang et al. 2017). Significant positive geopotential height anomalies occur in the region where the climatological trough is located over the WNP (Fig. 6b), and the trough is weakened considerably (Fig. 7b) in the negative phase. In the meantime, the WPSH is intensified significantly, with a southward-migrating ridge (Fig. 7b). The western edge of the 3160-gpm surface leans

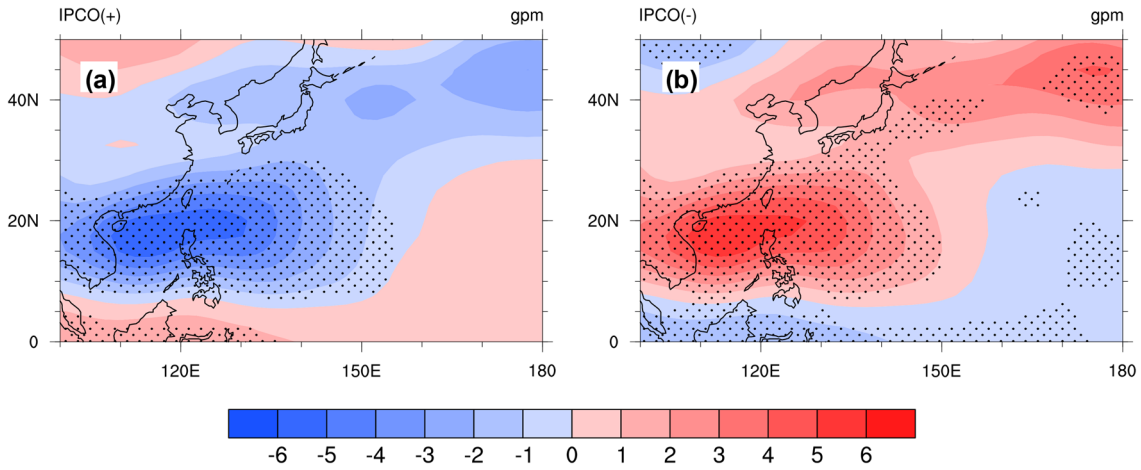

Fig. 6 Composite maps of geopotential height anomalies over the WNP in the boreal extended summer for the period 1979–2015 at the 700-hPa level. **a** The positive intra-seasonal IPCO phase; **b** the negative intra-seasonal IPCO phase. The shaded areas denote geopotential height (units: gpm), the stippled regions significant above the 99% confidence levels using Student's *t*-test

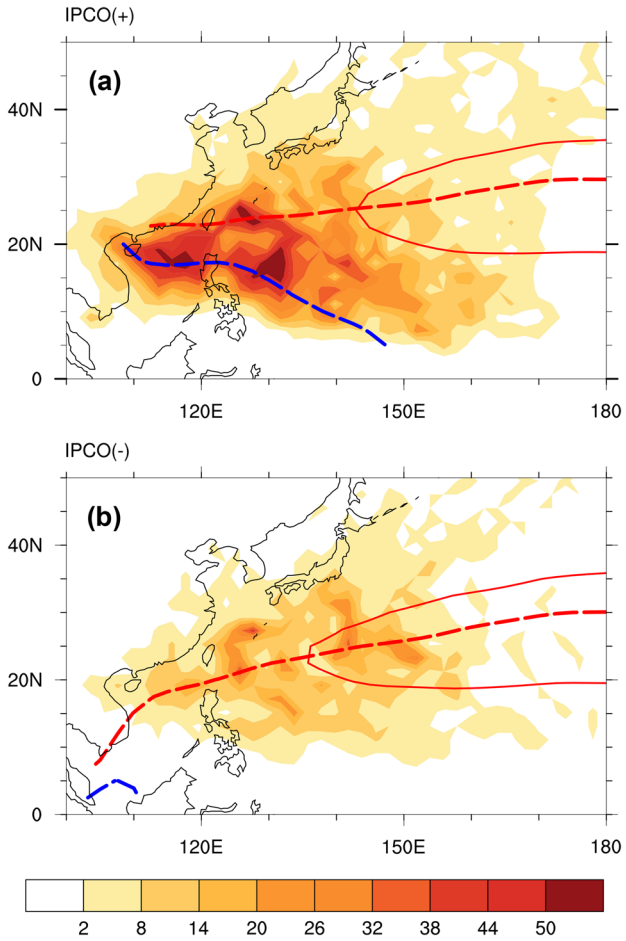

Fig. 7 Frequency of TCs occurrence in each 2° latitude × 2° longitude grid over the WNP in the boreal extended summer for the period 1979–2015. **a** The positive intra-seasonal IPCO phase; **b** the negative intra-seasonal IPCO phase. The shaded areas indicate frequency of TCs occurrence. Dashed lines the trough (blue) and WPSH ridge (red), respectively. Solid line the 3160 gpm isoline of geopotential height

farther to the west. It is clear that the intensified WPSH results in anomalously anticyclonic circulation at low latitudes and west of 150°E in the WNP (Fig. 8b). Powerful westward and northwestward steering flow in the WNP south of 10°N and west of 140°E, supporting the westward and northwestward motion of TCs in these regions. However, there are only a few of TCs in these area. To the region between 10°N and 25°N and east of 130°E, anomalously southward and southeastward flows can prevent TCs from moving to north and northeast at first, but when the TCs move to the north of 20°N and west of 135°E, anomalous westerlies can also prevent TCs from moving to west and northwest and reaching the Indo-China Peninsula, eastern coastal China, and islands in the SCS. Also, as can be seen from Fig. 7b, the WPSH is so strong, there is an intensified north–south ridge of the WPSH south of 20°N in the WNP, it can also keep TCs from moving to west and northwest. These features lead to most TC tracks tend to recurve to northeastward and northward in the negative phase.

4.2 Energy conversion

Actually, the essence of steering flow is the result of energy transformation. It is useful to study the impact of steering flow on TC tracks from the perspective of energy conversion. The atmosphere is not an isolated system: it exchanges energy with its surroundings, and loses kinetic energy by friction. The existing kinetic energy is kept within 10 days. Consequently, external energy input is needed to drive the movement of the atmosphere; however, solar radiation, as the major external source of energy, cannot be converted into kinetic energy directly, it need to be converted to PPE firstly. As shown in Eq. 7, it is clear that diabatic heating (G) is the major energy source of PPE other than energy redistribution within the atmospheric system. Latent heat provides the major part of the diabatic heating in the tropics. Given that the specific cloud liquid water content is an approximate

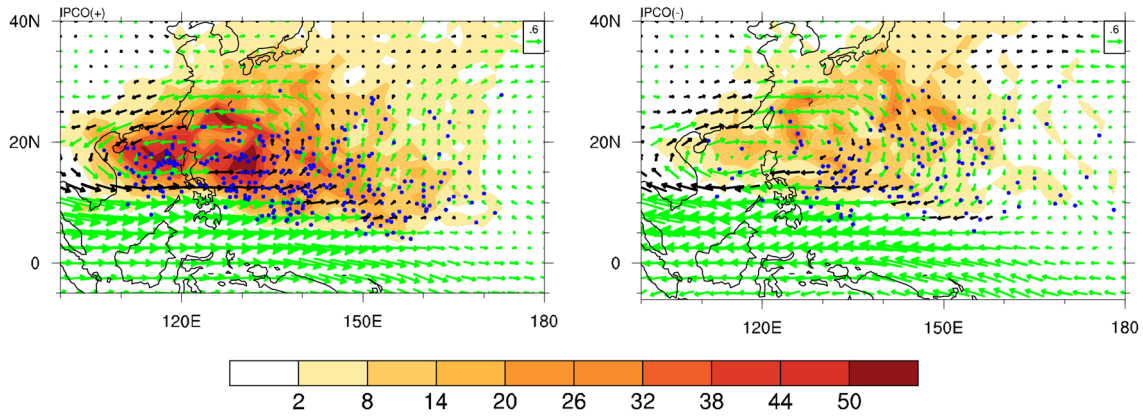

Fig. 8 As in Fig. 6, but for horizontal wind at 700-hPa. The green vectors (units: m/s) indicate significant above the 99% confidence level. Blue tiny dots show TC genesis location. Shaded areas indicate frequency of TCs occurrence in each 2° latitude × 2° longitude grid

measure of the available latent heat, we analyze the specific cloud liquid water content at 700 hPa in the positive and negative intra-seasonal IPCO phases.

When the intra-seasonal IPCO is in its positive phase, there are positive anomalies of cloud liquid water content at 10°−25°N (Fig. 9a), especially in the region where the climatological trough is located. This indicates the release of more latent heat of condensation and therefore an increased accumulation of PPE_1 compared with climatology. Positive anomalies of PPE_1 occur in the region of the climatological trough (Fig. 10a); however, although positive anomalies of cloud liquid water content also occur at middle and high latitudes in the positive phase over the WNP, anomalies of PPE_1 are negative, so less PPE_1 is released in these regions than normal (Fig. 10a). The possible reason is that G is composed of latent heat net flux, sensible heat net flux, net longwave radiation and net shortwave radiation, here, we just talk about latent heat net flux. To latent heat, it is the major part of the G in the tropics, but it is not true for the subtropics because of the influence of downdrafts and westerlies. Positive anomalies of cloud liquid water content can not enough to represent that more PPE_1 is released in the subtropics. Hence, less PPE_1 is accumulated at middle and high latitudes can be understood. From Eqs. 7 and 8, it is clear that energy can be converted from PPE_1 to PKE. The more PPE_1 is released, the more energy is converted to PKE. In Fig. 11a, in the trough region, more PKE is created than normal, which enhances the cyclonic circulation at lower latitudes over the WNP and intensifies the trough, leading to stronger westward and northwestward steering flow between 20°N and 30°N. In the climatological WPSH region, the conversion from PPE_1 to PKE is suppressed, which means the WPSH is weakened,

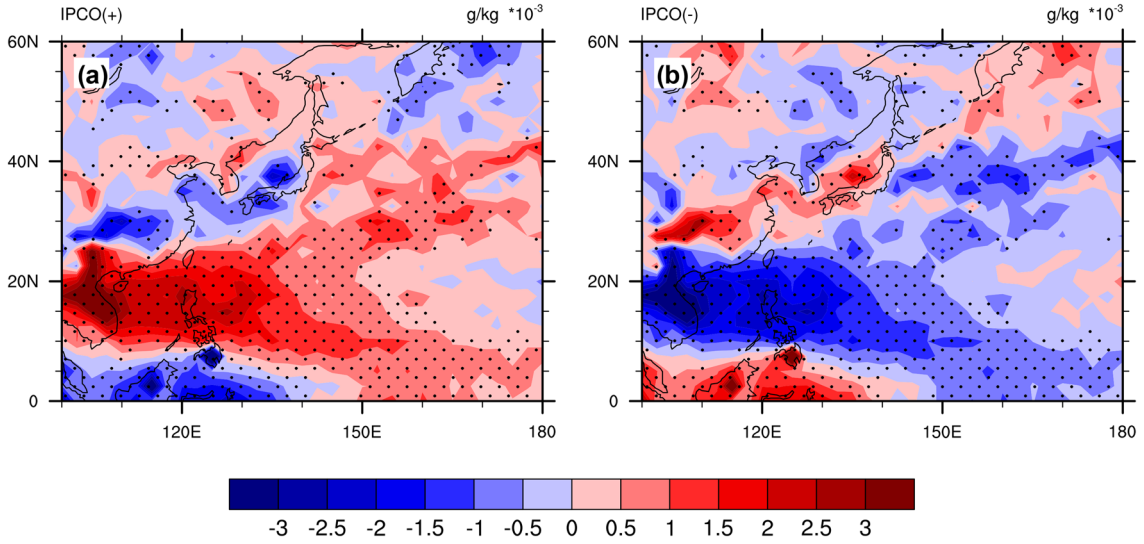

Fig. 9 As in Fig. 6, but for specific cloud liquid water content anomalies (units: g/kg) at the 700-hPa level

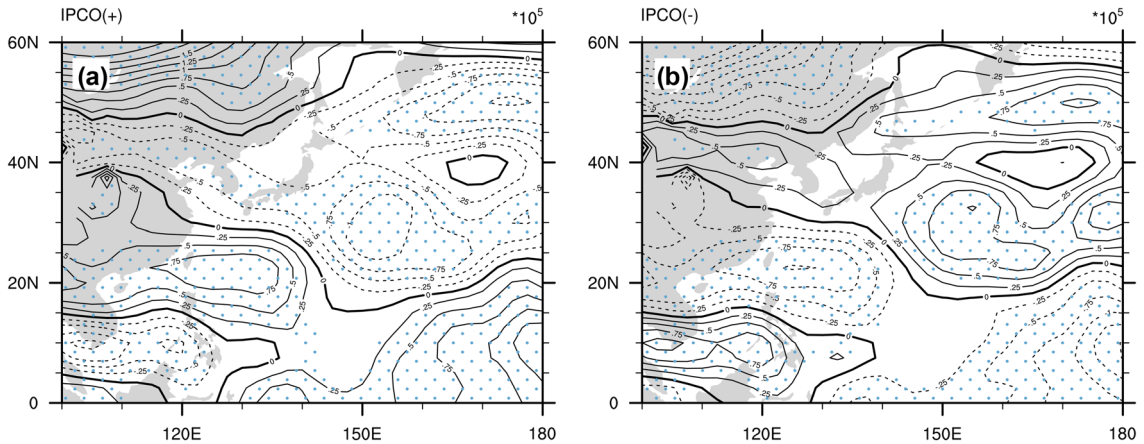

Fig. 10 As in Fig. 6, but for perturbation potential energy anomalies (units: J/m^2) at the 700-hPa level

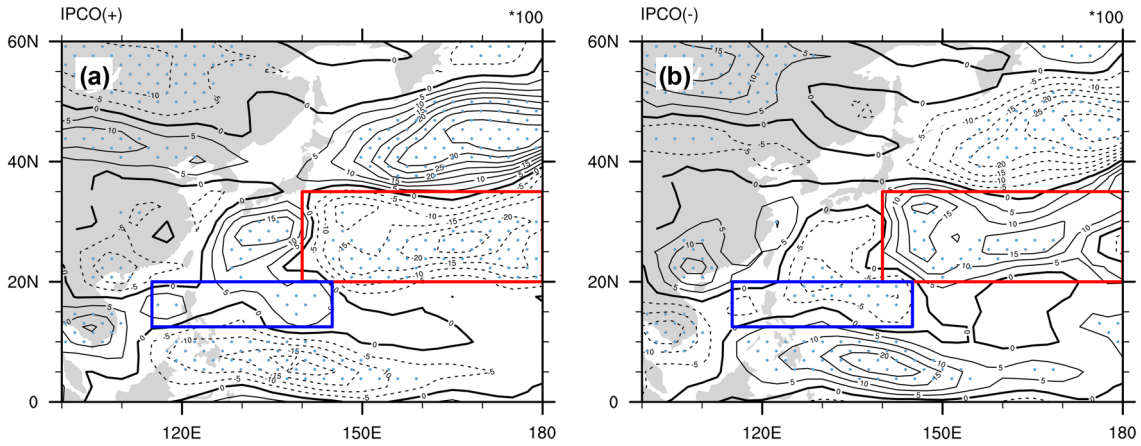

Fig. 11 As in Fig. 6, but for perturbation kinetic energy anomalies (units: J/m^2) at the 700-hPa level. The red (blue) box are the locations of the climatic western Pacific subtropical high (tough), respectively

reducing the effect of the steering flow caused by the WPSH in this region. Consequently, most TCs move westward and northwestward in the positive intra-seasonal IPCO phase.

The reverse is true in the negative intra-seasonal IPCO phase. Lower cloud liquid water content results in less PPE_1 being accumulated in the climatological trough region than normal (Figs. 9b, 10b), further decreasing the efficiency of conversion from PPE_1 to PKE (Fig. 11b). This weakens the cyclonic circulation at lower latitudes over the WNP, further suppressing the development of the trough. Therefore, anomalous southwesterlies and easterlies between 15°N and 30°N and east of 130°E in the WNP are strengthened with a weakening trough, and the westward and northwestward steering flows are suppressed. Following the same reasoning as used for the positive phase, negative anomalies of cloud liquid water content occur at middle and high latitudes over the WNP, less latent heat can not enough to suggests that less PPE_1 is used to support the development of the WPSH than normal, more PPE_1 are accumulated in the climatological WPSH region because of other energy sources, further enhancing the conversion efficiency from PPE_1 to PKE, thereby intensifying the WPSH and resulting in stronger steering flow. This then supports the initial westward and northwestward motion of TCs on the southern flanks of the WPSH; however, anomalous southwesterlies and easterlies in the west of WNP will prevent TCs from moving westward and northwestward. Consequently, most TC tracks turn northeastward and northward in the negative intra-seasonal IPCO phase.

4.3 Energy propagation

Energy is not static, it propagates through waves. The group velocity represents the velocity at which wave energy propagates. Previous studies paid more attention to the direct effect of wave on TC genesis location instead of tracks (e.g Molinari et al. 1997; Huang and Chen 2007). To further understand how the wave energy disperses, Rossby wave ray tracing in horizontal non-uniform basic flow at 700 hPa is presented in Fig. 12. In the positive intra-seasonal IPCO phase (Fig. 12a), the Rossby wave rays emanating from the convective center of the intra-seasonal IPCO in the WNP ($Wave_{WNP}$) propagate into the region of the climatological trough, and intensify the development of anomalously cyclonic circulation, thereby supporting the development of the trough. This leads to stronger westward and northwestward steering airflow north of 20°N. Moreover, some eastward Rossby wave rays that are excited at the convective center of the intra-seasonal IPCO in the EEIO ($Wave_{EEIO}$) arrive in the WNP, and intensify the trough, further enhancing the westward and northwestward steering airflow north of 20°N. As a result, the number of straight west- and northwest-moving TC tracks sharply increases in the WNP. In the negative intra-seasonal IPCO phase (Fig. 12b), the westward-moving $Wave_{WNP}$ divides into two apparently distinct branches about 10 days later. One branch continues to spread to the west, propagating to the EEIO, while the other turns northeastward and northward, which favors northeastward motion of TCs over the WNP. Meanwhile, the few northeastward-moving $Wave_{EEIO}$ reach the southern Indo-China Peninsula, which results in an intensified north–south ridge of the WPSH, further suppressing the westward motion of TCs and leading to fewer straight west- and northwest-moving TC tracks in the negative phase.

5 Summary and discussion

This study investigates the TC tracks in different intra-seasonal IPCO phases over the WNP. When the intra-seasonal IPCO is in its positive phase, the number of straight west- and

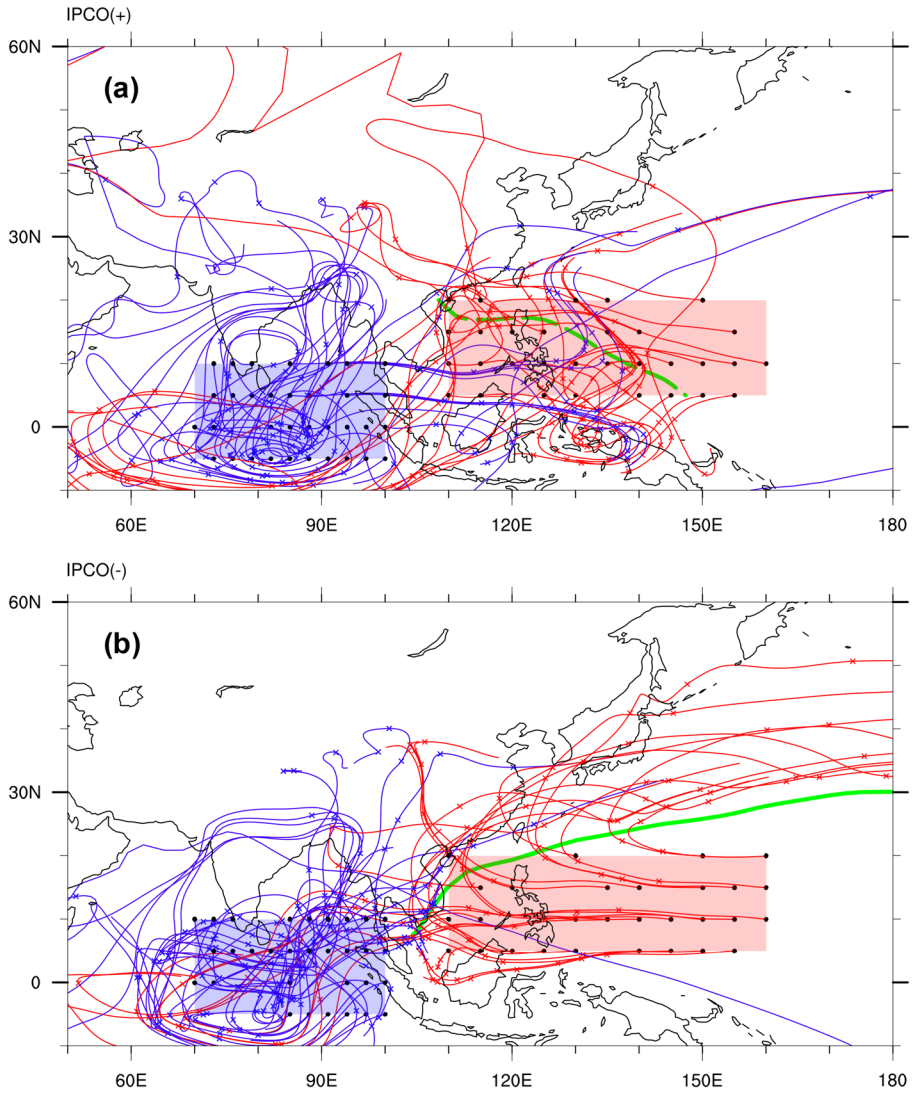

Fig. 12 The nonstationary Rossby wave trajectories [red (blue) curves: wave sources locate in the WNP (EEIO)] in horizontal non-uniform basic flow at the 700-hPa level in the boreal extended summer for the period 1979–2015. **a** The positive intra-seasonal IPCO phase; (b) the negative intra-seasonal IPCO phase. The black dots represent the initial position of the disturbances (a virtual wave source), and the crosses 5 days' interval. The boxes the EEIO (blue), the WNP (red), respectively

northwest-moving tracks sharply increases. When the intra-seasonal IPCO is in its negative phase, recurving TC tracks account for a larger proportion. The results are similar to the previous study (Kim et al. 2008). In their studies, they pointed that when the MJO-related convection center is found in the equatorial Indian Ocean (the tropical WNP), a dense area of tracks migrates eastward (westward). These features imply that there is closely connection between the traditional MJO and propagating part of the intra-seasonal IPCO in the boreal extended summer. And it also further verify the reliability of this study. But the evident difference can be found in the total number. Not only that, the differences in TC genesis numbers, locations and tracks are also obvious in single quadrant. Moreover, in their study, although they discussed TC tracks characters qualitatively in different periods (June–September, June-July, August–September), but they did not give a detail statistics characters of TC tracks. And they analyzed the possible physical mechanisms from a perspective of steering flows. However, in our study, we examined the modulation of the intra-seasonal IPCO on tropical cyclone tracks quantitatively, and to the part of possible mechanisms, we not only focus on steering flows but also energy conversion and transmission.

Figure 13 displays schematic diagram of modulation of tropical cyclone tracks over the WNP by the intra-seasonal IPCO. In the positive phase of the intra-seasonal IPCO, more PPE_1 are converted into PKE in the climatological trough region, which intensifies the trough so that it spreads farther east. Meanwhile, the energy transmitted by the $Wave_{WNP}$ and $Wave_{EEIO}$ further deepens the tough. In the climatological WPSH region, the conversion from PPE_1 to PKE is suppressed, which means the WPSH is weakened, thereby reducing the effect of the steering flow associated with the WPSH in this region. These features lead to an anomalously cyclonic circulation. On the one hand, to the regions where TCs mainly generate, there are not significant

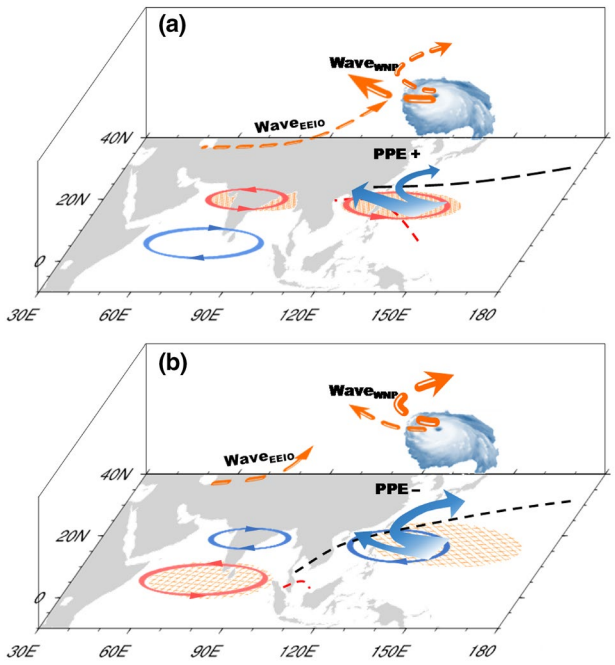

Fig. 13 Schematic diagram of modulation of tropical cyclone tracks over the WNP by intra-seasonal IPCO in the positive (**a**) and negative (**b**) intra-seasonal IPCO phases. Orange shadings represent main TC generating areas. Orange vector lines indicate the travel directions of the Rossby wave. Black (red) dashed lines show the ridge of WPSH (trough). Blue and red circulation lines represent anomalously anticyclonic and cyclonic circulations, respectively. Blue vector lines indicate TC tracks. PPE+ (PPE−) indicate positive (negative) PPE anomalies

change of circulation, hence, most TCs move westward and northwestward because of β-effect. On the other hand, anomalously westward airflow about 10° poleward of 20°N prevent a northward and northeastward shift when the TCs move to the north of 20°N and west of 150°E. Hence, most TCs move westward and northwestward. In the negative phase of the intra-seasonal IPCO, the conversion from PPE_1 to PKE is suppressed at lower latitude and the trough is sharply weakened. In contrast, more PPE_1 converts to PKE in the WPSH region, and the WPSH is intensified with a southward extending ridge. The energy transmitted by the $Wave_{EEIO}$ intensifies the ridge of the WPSH over the south Indo-China Peninsula, which suppresses the westward and northwestward steering flow. Moreover, many $Wave_{WNP}$ turn northeastward and northward in the WNP, enhancing the northeastward steering flow. Consequently, most TC tracks move northeastward and northward.

Previous studies on the physical mechanisms of TC tracks have focused on a single layer. To TC tracks, steering flow must have a common direction on all levels. To verify the applicability of PPE_1 and nonstationary Rossby wave ray tracing to the study of TC tracks, we also examine the representation of PPE_1 and Rossby wave ray tracing in the vertical direction. The results are in agreement with those in Sect. 4 (figures not shown). Hence, atmospheric PPE and non-stationary Rossby wave ray tracing in the horizontal non-uniform basic flow are powerful tools for studying TC activity. Combining these methods with the intra-seasonal IPCO shows great promise for forecasting TC activity; however, we have only discussed TC activity over the WNP in this work. Further work is required to investigate whether these two methods apply to TC activities in other basins.

Acknowledgements The authors are deeply indebted to Lidou Huyan and Quanjia Zhong for their helpful comments and suggestions. This work was jointly supported by the National Natural Science Foundation of China (NSFC, 41530424) project, State Oceanic Administration (SOA) International Cooperation Program on Global Change and Air–Sea Interactions (GASI-IPOVAI-03) and the Fundamental Research Funds for the Central Universities of China (312231103).

Appendix A

The governing equations of the atmospheric layer PPE_1

The governing equations of the atmospheric layer PPE_1 $\left(\hat{P}'_{a1},\ \hat{P}'_{a1} = \left\langle C_p T' \right\rangle\right)$ and perturbation kinetic energy (PKE, K') are derived as follows (Wang et al. 2012):

$$\left\{ \left\langle \frac{\partial \hat{P}'_{a1}}{\partial t} \right\rangle \right\} = -VF_{PE} + C_k - HFB_{PE} + G, \tag{7}$$

$$\left\{ \left\langle \frac{\partial K'}{\partial t} \right\rangle \right\} = -VF_K - C_k + D - HFB_K, \tag{8}$$

where $K' = K - \bar{K}$ and $\overline{(\,)}$ is the global average; $\overline{(\,)} = \frac{1}{4\pi a^2} \int_{-\frac{\pi}{2}}^{\frac{\pi}{2}} \int_0^{2\pi} (\,) d\lambda d\varphi$, where φ is latitude and λ longitude; $\langle\rangle = \frac{1}{g} \int_{p_1}^{p_2} \cdot dp$; $\{\}$ represents a horizontal integration with $\{\} = \iint_\sigma d\sigma$, where $d\sigma = a^2 \cos\varphi d\lambda d\varphi$; a is the Earth's radius; VF_{PE} and VF_K are vertical fluxes of PPE_1 and PKE, respectively; $VF_{PE} = \left\{ \left\langle \frac{\partial}{\partial p} \left(\omega \hat{P}'_{a1} - \overline{\omega \hat{P}'_{a1}} \right) \right\rangle \right\}$; $VF_K = \left\{ \left\langle \frac{\partial}{\partial p} \left(\omega K - \overline{\omega K} \right) - \frac{\partial}{\partial p} \left(\omega \Phi - \overline{\omega \Phi} \right) \right\rangle \right\}$, where ω is the vertical velocity in terms of the pressure coordinate; and $C_k = \left\{ \left\langle \omega\alpha - \overline{\omega\alpha} \right\rangle \right\}$ represents the energy conversion between PPE_1 and PKE, where α is the air specific volume. When $C_k < 0$, PPE_1 is converted to PKE, whereas when $C_k > 0$, PKE is converted to PPE_1. $G = \left\{ \left\langle Q - \bar{Q} \right\rangle \right\}$ represents the PPE tendency associated with diabatic heating of the atmosphere, where Q is the atmospheric diabatic heating rate. HFB_{PE} and HFB_K are the horizontal boundary fluxes of PPE_1 and PKE, respectively, with $HFB_{PE} =$

$\left\{\left\langle \nabla_h \cdot \left(\vec{V}_h \hat{P}'_{a1}\right)\right\rangle\right\}$ and $HFB_K = \left\{\left\langle \nabla_h \cdot \left(\vec{V}_h K\right)\right\rangle + \left\langle \nabla_h \cdot \left(\vec{V}_h \Phi\right)\right\rangle\right\}$, where the horizontal wind velocity $\vec{V}_h = u\vec{i} + v\vec{j}$; u and v are the zonal and meridional components of horizontal wind velocity, respectively; ∇_h is the horizontal gradient operator; $\nabla_h = \frac{1}{a\cos\varphi}\frac{\partial}{\partial\varphi}\vec{i} + \frac{1}{a}\frac{\partial}{\partial\varphi}\vec{j}$; Φ is geopotential; and D represents viscous dissipation, with$D = \left\{\left\langle \vec{V}_h \cdot \vec{F}_h - \overline{\vec{V}_h \cdot \vec{F}_h}\right\rangle\right\}$, where $\vec{F}_h$ is the horizontal friction term.

Appendix B

Non-stationary Rossby wave ray tracing method in the horizontal non-uniform basic flow

Previous research has suggested that the barotropic vorticity equation is a useful tool to describe Rossby wave propagation (Hoskins and Karoly 1981; Branstator 1983; Hoskins and Ambrizzi 1993). By employing the Mercator projection, the perturbation method, and the Wentzel–Kramers–Brillouin (WKB) approximation, it is possible to obtain a linearized barotropic non-divergent vorticity equation in spherical coordinates (Eq. 9) and dispersion relation (Eq. 10) (Hoskins and Karoly 1981; Li and Li 2012; Li et al. 2015):

$$\left(\frac{\partial}{\partial t} + \bar{u}_M\frac{\partial}{\partial x} + \bar{v}_M\frac{\partial}{\partial y}\right)\nabla_M^2\psi' + \bar{q}_y\frac{\partial\psi'}{\partial x} - \bar{q}_x\frac{\partial\psi'}{\partial y} = 0, \quad (9)$$

$$\omega = \bar{u}_M k + \bar{v}_M l + \frac{\bar{q}_x l - \bar{q}_y k}{K^2}, \quad (10)$$

where ψ is the stream function; $\bar{u}_M = \frac{\bar{u}}{\cos\varphi}$ and $\bar{v}_M = \frac{\bar{v}}{\cos\varphi}$ are the zonal and meridional components of the basic flow in a Mercator projection, respectively; $\bar{q} = \frac{\nabla_M^2\bar{\psi}}{\cos^2\varphi} + 2\Omega\sin\varphi$ is the fundamental quantity of absolute vorticity; $K^2 = l^2 + k^2$ is the total wavenumber, where k and$l$ are the zonal and meridional wavenumbers, respectively; and ω is the angular frequency.

The ray path is a trajectory locally tangent to the group velocity vector (Lighthill 1978). Hence, Li and Li (2012) detected the energy dispersion by calculating the ray trajectories, further revealing the impact of meridional basic flow on the wave propagation:

$$f(l) = \bar{v}_M l^3 + k\left(\bar{u}_M - c_x\right)l^2 + \left(k^2\bar{v}_M + \bar{q}_x\right)l + \left[k^2\left(\bar{u}_M - c_x\right) - \bar{q}_y\right]k = 0, \quad (11)$$

where $\mathbf{c} = (c_x, c_y)$ is the phase velocity.

The zonal and meridional components of group velocity, u_g and v_g, respectively, take the form

$$u_g = \left(1 + \frac{1}{1+l^2}\right)\bar{u}_M + \frac{l}{1+l^2}\bar{v}_M - \frac{l}{1+l^2}\frac{l}{k} - \frac{l\left(\bar{q}_x + l\bar{q}_y\right)}{k^2\left(1+l^2\right)^2}, \quad (12)$$

$$v_g = \frac{l}{1+l^2}\bar{u}_M + \left(1 + \frac{l^2}{1+l^2}\right)\bar{v}_M - \frac{l^2}{1+l^2}\frac{\omega}{l} - \frac{\bar{q}_x + l\bar{q}_y}{k^2\left(1+l^2\right)^2}. \quad (13)$$

Due to the longitudinal and latitudinal variation of the basic state, l, k, and θ (phase) change along the ray paths. Their evolution is determined by kinematic wave theory (Whitham 1960) as follows:

$$\frac{d_g k}{dt} = -\frac{\partial\omega}{\partial x} = -k\frac{\partial\bar{u}_M}{\partial y} - l\frac{\partial\bar{v}_M}{\partial x} + \frac{\bar{q}_{xy}k - \bar{q}_{xx}l}{K^2}, \quad (14)$$

$$\frac{d_g l}{dt} = -\frac{\partial\omega}{\partial y} = -k\frac{\partial\bar{u}_M}{\partial y} - l\frac{\partial\bar{v}_M}{\partial x} + \frac{\bar{q}_{yy}k - \bar{q}_{xy}l}{K^2}, \quad (15)$$

$$\frac{d_g\theta}{dt} = \frac{\partial\theta}{\partial t} + \mathbf{c_g}\cdot\nabla\theta, \quad (16)$$

where $\frac{d_g}{dt} = \frac{\partial}{\partial t} + u_g\frac{\partial}{\partial x} + v_g\frac{\partial}{\partial y}$ denotes the Lagrangian variation moving at the group velocity; $\mathbf{c_g} = \left(u_g, v_g\right)$ is local group velocity. Therefore, the ray trajectory and phase evolution can be integrated through Eqs. (14)–(16) using Runge–Kutta methods if the basic and initial states are known.

References

Branstator G (1983) Horizontal energy propagation in a barotropic atmosphere with meridional and zonal structure. J Atmos Sci 40:1689–1708

Camargo SJ, Sobel AH (2005) Western North Pacific tropical cyclone intensity and ENSO. J Clim 18:2996–3006

Chan JCL (1995) Tropical cyclone activity in the western North Pacific in relation to the stratospheric Quasi-Biennial oscillation. Mon Weather Rev 123:2567–2571

Chan JCL (2010) Movement of tropical cyclones. In: Chan JCL, Kepert JD (eds) Global perspectives on tropical cyclones, 4th edn. World scientific, Singapore, p 133

Chen TC, Wang SY, Yen MC, Clark AJ (2009) Impact of the intraseasonal variability of the western North Pacific large scale circulation on tropical cyclone tracks. Weather Forecast 24:646–666

Choi KS, Cha YM, Kim HD, Kang SD (2016) Possible influence of western North Pacific monsoon on TC activity in mid-latitudes of East Asia. Clim Dyn 46:1–13

Dee DP, Uppala SM, Simmons AJ, Berrisford P, Poli P, Kobayashi S, Andrae U, Balmaseda MA, Balsamo G, Bauer P, Bechtold P, Beljaars ACM, van de Berg L, Bidlot J, Bormann N, Delsol C, Dragani R, Fuentes M, Geer AJ, Haimberger L, Healy SB,

Hersbach H, Holm EV, Isaksen L, Kallberg P, Kohler M, Matricardi M, McNally A, Monge-Sanz BM, Morcrette JJ, Park BK, Peubey C, de Rosnay P, Tavolato C, Thepaut JN, Vitart F (2011) The ERA-interim reanalysis: configuration and performance of the data assimilation system. Q J Roy Meteor Soc 137:553–597

Ding RQ, Li JP, Seo K-H (2011) Estimate of the predictability of boreal summer and winter intra-seasonal oscillations from observations. Mon Weather Rev 139:2421–2438

Dong D, Li JP, Huyan LD, Xue JQ (2017) Atmospheric energetics over the tropical pacific during the ENSO Cycle. J Clim 30:3635–3654

Emanuel K (2003) Tropical cyclones. Annu Rev Earth Planet Sci 31:75–104

Emanuel K (2005) Increasing destructiveness of tropical cyclones over the past 30 years. Nature 436:686–688

Gao L, Li JP (2007) Progress in the study of atmospheric energy efficiency (in Chinese). Adv Earth Sci 22:486–494

Gao L, Li JP (2012) Relationship and mechanism between perturbation potential energy and atmospheric general circulation anomalies. Chin J Geophys 55:359–374

Gao L, Li JP, Ren HL (2006) Some characteristics of the atmosphere during an adiabatic process. Prog Nat Sci (Chinese Edition) 16:644–648

Gray WM (1979) Hurricanes: their formation, structure, and likely role in the tropical circulation. In: Shaw DB (ed) Meteorology over the tropical oceans, pp 155–218

Harr PA, Elsberry RL (1991) Tropical cyclone track characteristics as a function of large-scale circulation anomalies. Mon Weather Rev 119:1448–1468

Harr PA, Elsberry RL (1995) Large-scale circulation variability over the tropical western North Pacific. Part I: spatial patterns and tropical cyclone characteristics. Mon Weather Rev 123:1225–1246

Hartmann DL, Maloney ED (2001) The Madden–Julian oscillation, barotropic dynamics, and North Pacific tropical cyclone formation. Part II: stochastic barotropic modeling. J Atmos Sci 58:2559–2570

Hoskins BJ, Ambrizzi T (1993) Rossby-wave propagation on a realistic longitudinally varying flow. J Atmos Sci 50:1661–1671

Hoskins BJ, Karoly DJ (1981) The steady linear response of a spherical atmosphere to thermal and orographic forcing. J Atmos Sci 38:1179–1196

Huang RH, Chen GH (2007) Research on interannual variations of tracks of tropical cyclones over northwest Pacific and their physical mechanism. Acta Meteorol Sin (in Chinese) 65:683–694

Kalnay E, Kanamitsu M, Kistler R, Collins W, Deaven D, Gandin L, Iredell M, Saha S, White G, Woollen J, Zhu Y, Chelliah M, Ebisuzaki W, Higgins W, Janowiak J, Mo KC, Ropelewski C, Wang J, Leetmaa A, Reynolds R, Jenne R, Joseph D (1996) The NCEP/NCAR 40-year reanalysis project. B Am Meteorol Soc 77:437–471

Kikuchi K, Wang B, Kajikawa Y (2012) Bimodal representation of the tropical intra-seasonal oscillation. Clim Dyn 38:1989–2000

Kim JH, Ho CH, Kim HS, Sui CH, Park SK (2008) Systematic variation of summertime tropical cyclone activity in the western north pacific in relation to the madden-julian oscillation. J Clim 21:1171–1191

Kim JS, Kim ST, Wang L, Wang X, Moon YI (2016) Tropical cyclone activity in the northwestern Pacific associated with decaying Central Pacific El Ninos. Stoch Environ Res Risk Assess 30:1335–1345

Knutson TR, McBride JL, Chan J, Emanuel K, Holland G, Landsea C, Held I, Kossin JP, Srivastava AK, Sugi M (2010) Tropical cyclones and climate change. Nat Geosci 3:157–163

Lau KM, Chan PH (1986) Aspects of the 40–50 day oscillation during the northern summer as inferred from outgoing longwave radiation. Mon Weather Rev 114:1354–1367

Li JP, Gao L (2006) Theory on perturbation potential energy and its applications-concept, expression and spatiotemporal structures of perturbation potential energy (in Chinese). Chin J Atmos Sci 30:834–848

Li YJ, Li JP (2012) Propagation of planetary waves in the horizontal non-uniform basic flow. Chin J Geophys (in Chinese) 55:361–371

Li RCY, Zhou W (2013) Modulation of Western North Pacific tropical cyclone activity by the ISO. Part II: tracks and landfalls. J Clim 26:2919–2930

Li Y, Li J, Feng J (2012) A teleconnection between the reduction of rainfall in southwest western Australia and North China. J Clim 25(24):8444–8461

Li YJ, Li JP, Feng J (2013) Boreal summer convection oscillation over the Indo-Western Pacific and its relationship with the East Asian summer monsoon. Atmos Sci Lett 14:66–71

Li YJ, Li JP, Jin FF, Zhao S (2015) Interhemispheric propagation of stationary rossby waves in a horizontally nonuniform background flow. J Atmos Sci 72:3233–3256

Li JP, Swinbank R, Grotjahn R, Volkert H (2016a) Dynamics and predictability of large-scale, high-impact weather and climate events. Cambridge University Press, London

Li JP, Wang QY, Li YJ, Zhang JW (2016b) Review and perspective on the climatological research of tropical cyclones in terms of energetics (in Chinese). J Beijing Normal Univ (Natural Science) 52:705–713

Li JP, Zhao S, Li YJ, Wang L, Sun C (2016c) On the role of perturbation potential energy in variability of the East Asian summer monsoon: current status and prospects (in Chinese). Adv Earth Sci 31:115–125

Lighthill J (1978) Wave in fluids. Cambridge University Press, London

Lorenz EN (1955) Available potential energy and the maintenance of the general circulation. Tellus 7:157–167

Maloney ED, Hartmann DL (2000a) Modulation of eastern North Pacific hurricanes by the Madden-Julian oscillation. J Clim 13:1451–1460

Maloney ED, Hartmann DL (2000b) Modulation of hurricane activity in the Gulf of Mexico by the Madden-Julian oscillation. Science 287:2002–2004

Margules M (1903) Über die Energie der stürme. Jahrbuch. Zen-tralanstalt für. Meteorologie und Geodynamik, Wien, pp 1–26

Molinari J, Knight D, Dickinson M, Vollaro D, Skubis S (1997) Potential vorticity, easterly waves, and eastern Pacific tropical cyclogenesis. Mon Weather Rev 125:2699–2708

Oort AH, Ascher SC, Levitus S, Peixoto JP (1989) New estimates of the available potential-energy in the world ocean. J Geophys Res Oceans 94:3187–3200

Pyper BJ, Peterman RM (1998) Comparison of methods to account for autocorrelation in correlation analyses of fish data. Can J Fish Aquat Sci 55(9):2127–2140

Sharmila S, Walsh KJE (2017) Impact of large-scale dynamic versus thermodynamic climate conditions on contrasting tropical cyclone genesis frequency. J Clim 30:8865–8883

Smith PJ (1969) On the contribution of a limited region to the global energy budget. Tellus 21:202–207

Smith PJ, Vincent DG, Edmon HJ (1977) The time dependence of reference pressure in limited region available potential energy budget equations. Tellus 29:476–480

Sobel AH, Maloney ED (2000) Effect of ENSO and the MJO on western North Pacific tropical cyclones. Geophys Res Lett 27:1739–1742

Sun C, Li JP, Feng J, Xie F (2015) A decadal-scale teleconnection between the North Atlantic oscillation and subtropical eastern Australian rainfall. J Clim 28:1074–1092

Taylor KE (1979) Formulas for calculating available potential energy over uneven topography. Tellus 31:236–245

Wang B, Chan JCL (2002) How strong ENSO events affect tropical storm activity over the Western North Pacific. J Clim 15:1643–1658

Wang CZ, Wang X (2013) Classifying El Nino Modoki I and II by different impacts on rainfall in Southern China and Typhoon tracks. J Clim 26:1322–1338

Wang L, Li JP, Guo Y (2012) Governing equations of atmospheric layer perturbation potential energy and its applications, energy budget of the South China Sea summer monsoon activity (in Chinese). Chin J Atmos Sci 36:769–783

Wang X, Zhou W, Li CY, Wang DX (2014) Comparison of the impact of two types of El Nino on tropical cyclone genesis over the South China Sea. Int J Climatol 34:2651–2660

Wang QY, Li JP, Li YJ, Zhang JW (2018) Modulation of tropical cyclogenesis location and frequency over the Indo-western North Pacific by the intra-seasonal Indo-western Pacific convection oscillation during the boreal extended summer. J Clim 31:1435–1450

Wheeler MC, Hendon HH (2004) An all-season real-time multivariate MJO index: Development of an index for monitoring and prediction. Mon Weather Rev 132:1917–1932

Whitham GB (1960) A note on group velocity. J Fluid Mech 9(3):347

Xie YB (1978) Current status and future possible development of energetic synoptic analysis and prediction method. Meteorol Sci Technol 2:5–9

Xie F, Li JP, Tian WS, Zhang JK, Sun C (2014) The relative impacts of El Niño Modoki, canonical El Niño, and QBO on tropical ozone changes since the 1980s. Environ Res Lett 9:064020

Xue JQ, Li JP, Sun C, Zhao S, Mao JY, Dong D, Li YJ, Feng J (2018) Decadal-scale teleconnection between South Atlantic SST and southeast Australia surface air temperature in austral summer. Clim Dyn 50:2687–2703

Yang L, Du Y, Wang DX, Wang CZ, Wang X (2015) Impact of intra-seasonal oscillation on the tropical cyclone track in the South China Sea. Clim Dyn 44:1505–1519

Zhan RF, Wang YQ, Lei XT (2011a) Contributions of ENSO and East Indian Ocean SSTA to the interannual variability of Northwest Pacific tropical cyclone frequency. J Clim 24:509–521

Zhan RF, Wang YQ, Wu CC (2011b) Impact of SSTA in the East Indian Ocean on the frequency of Northwest Pacific tropical cyclones: a regional atmospheric model study. J Clim 24:6227–6242

Zhan RF, Wang YQ, Wen M (2013) The SST gradient between the Southwestern Pacific and the Western Pacific Warm Pool: a new factor controlling the Northwestern Pacific tropical cyclone genesis frequency. J Clim 26:2408–2415

Zhan RF, Wang YQ, Tao L (2014) Intensified impact of East Indian Ocean SST anomaly on tropical cyclone genesis frequency over the Western North Pacific. J Clim 27:8724–8739

Zhang JW, Li JP, Li YJ (2015) Intra-seasonal characteristics of the Indo-West Pacific convection oscillation. Chin J Atmos Sci (in Chinese) 39:221–234

Zhu BZ, Wang B (1993) The 30–60-day convection seesaw between the tropical Indian and western Pacific oceans. J Atmos Sci 50:184–199

Zhu CW, Nakazawa T, Li JP (2004) Modulation of tropical depression/cyclone over the Indian-Western Pacific oceans by Madden–Julian oscillation. Acta Meteorol Sin (in Chinese) 62:42–50